Mechanical properties of compliant composite particles effective in toughening glassy polymers

Mary E. Boyce, A. S. Argon and D. M. Parks
Massachusetts Institute of Technology, Cambridge, MA 02139, USA
(Received 11 August 1986; revised 18 December 1986; accepted 12 January 1987)

The mechanical properties of compliant composite particles incorporating block components of rubbery and glassy polymer phases, with two morphologies, different from that in high impact polystyrene (HIPS), have been studied in detail. By a combination of analytical and numerical modelling, it is demonstrated that block copolymer particles with the same volume fraction of rubber as HIPS are ineffective in craze nucleation when the rubbery component is dispersed in a topologically continuous glassy component, but are very much more effective when the two components are distributed in a concentric spherical shell morphology. These two morphologies achieve roughly upper and lower bounds to the stiffness of the particle. While thermal expansion misfit stresses make an important contribution to the stress state outside a particle, the main stress concentrating effectiveness of the particle comes from its increased tensile compliance. Analysis further shows that viscoplastic relaxation of the thermal stresses outside the particle improves its effectiveness somewhat, if such stress relaxation can produce proto-pores, that are the forerunners to craze initiation.

(Keywords: compliant particles; toughening; composite particles)

INTRODUCTION

The incorporation of rubbery particles into brittle glassy polymers has long been recognized to have the capacity to significantly toughen these materials. Bucknall and Smith identified the source of this toughness to be crazes that were initiated from the rubber particles[1]. Crazes will toughen a polymer only when they can be readily generated uniformly throughout the volume. The introduction of rubbery particles in the polymer serves the purpose of providing controlled sites for craze initiation in a quasi-homogeneous manner. If craze initiation is too difficult from surface stress concentrations in homogeneous glassy polymers, the average accompanying stress levels become too high. This results in premature fracture of craze matter, which then propagates through the material to general fracture. Thus, in homopolymers crazes act as precursors to fracture. This dual role of crazes as precursors for fracture and as sources of dilatational plasticity in glassy polymers has stimulated much research on the factors which influence the initiation, growth, and structure of crazes. These investigations have been extensively reviewed[2-5].

More recently, research utilizing block copolymers has been directed at understanding and controlling the various characteristics of the particles that influence the toughness of polymers through crazing, such as: particle chemistry, morphology, size and volume fraction[6,7]. In one such recent study of blending block copolymers of polybutadiene/polystyrene (PB/PS) together with additional low molecular weight PB to form composite particles with controllable morphology in high molecular weight PS, Gebizlioglu *et al.*[8,9] found dramatic improvement in toughness. Thus, the manner in which composite particles with different elastic and thermal expansion properties concentrate stress around them to initiate crazes needs to be understood. This need has been recognized by many investigators in the past. A summary of some early analysis of particles in HIPS is given by Bucknall[1]. Not considering many useful studies of spherical elastic heterogeneities in elastic media that abound in the materials science literature, there exist a number of more or less detailed studies specifically addressed to the properties of the composite particles in polymers that play a role in crazing[10-15]. An important aspect of the stress state around composite particles with a sizeable volume fraction of rubber is the thermal expansion misfit stresses that are built into the material as the polymer comes to room temperature from a processing excursion from around the glass transition temperature of the matrix phase. This important aspect has been recognized by a number of authors[7,9,11,14,15], although the consequences have been interpreted at times quite differently. While most of the analyses have considered particles only in infinite bodies, the effect of particle interaction in a tensile field have also been considered by Broutman and Panizza[16] in a finite element study.

Here, we will present the results of a combined finite element and analytical study of the interaction of spherical composite elastic particles with their viscoplastic surroundings, under a distant tensile stress. The analysis will range from considerations of particles in infinite fields to substantial volume fractions where particle interactions, due to both thermal misfit and the distant tensile field, become important and must be taken into account.

MORPHOLOGIES AND STRESS HISTORIES

Morphologies

Composite particles in high impact polystyrene (HIPS)

0032-3861/87/101680-15$03.00

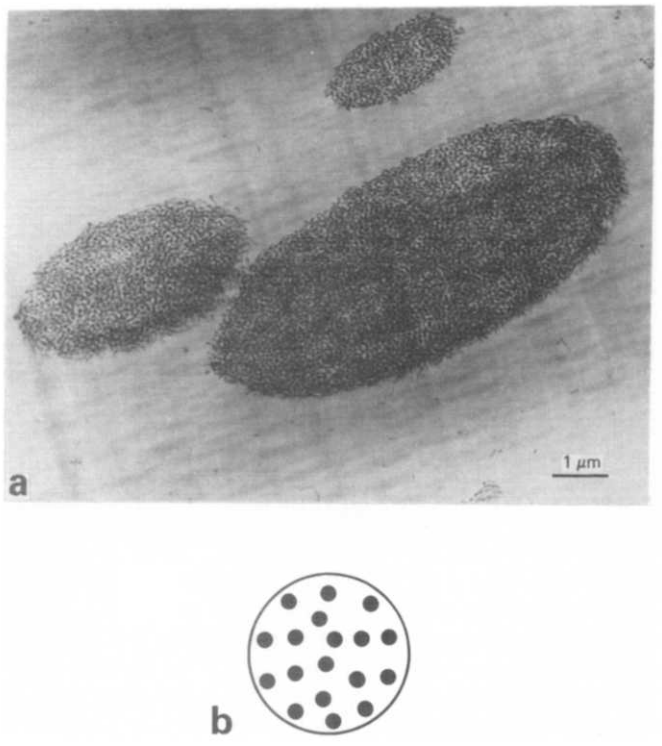

Figure 1 A KRO-1 resin particle: (a) micrograph, (b) equivalent morphology chosen to evaluate 'homogenized' elastic properties

consist of a collection of occluded stiff PS spheres in a topologically continuous minority phase of compliant polybutadiene (PB), generally produced by utilizing graft copolymers. Particles in acrylonitrile–butadiene–styrene (ABS) have the same general morphology as HIPS, but have a different blend of rubbers making up the topologically continuous compliant phase in the particles. Other particle morphologies consisting of core–shell arrangements where the compliant phase surrounds a central core of a single occluded particle of the stiff matrix phase[17], those of concentric spherical shell arrangement of alternating layers of stiff and compliant phases[18], and morphologies of more complex types[18], have been produced and partially explored[19]. All particles resulting from direct polymerization reactions or from solvent processing are spherical in geometry. They may be of greatly different sizes and size ranges.

Here, we will consider in some detail five different generic particle morphologies in heterogeneous polymers, and analyse their elastic properties in a viscoplastic matrix for the purpose of understanding their effectiveness in governing (dilatational) craze plasticity. These five morphologies include a pure PB/PS block copolymer particle with a morphology of tortuous and occasionally interconnected PB rods in a topologically continuous PS block phase; a pure PB particle; and two concentric spherical shell particles with alternating layers of PB and PS. The fifth morphology is that of the HIPS particle. The first of these particles has been obtained by Gebizlioglu *et al.*[8] by solution blending of KRO-1 resin into PS. The second is an idealized particle that is likely to represent the ultimate achievable properties. The third and fourth morphologies are also of a morphology achieved by Gebizlioglu *et al.*[9] in ternary blends of KRO-1 resin with low molecular weight PB into PS. They differ only in the thickness of the PB layer between the PS layers. Since the first two morphologies are either quasi-random, or isotropic, they will be analysed by first obtaining composite average elastic properties and thermal expansion coefficients for the inner morphology of the particle and then treating the particle as 'homogenized' and isotropic in a background glassy PS matrix. In this sense, the approach lends itself directly to the HIPS particle morphology which will be evaluated last.

The first of the four morphologies to be discussed will be referred to as the 'homogenized' particle. More specifically, the particle of interest is made by dispersing KRO-1 resin with a tortuously wavy rod morphology of 23 wt% block PB in a topologically continuous block phase of PS, making up a spherical particle in a majority phase of high molecular weight PS, as shown in *Figure 1a*. Since the PB rods are randomly oriented inside the composite particle, the elastic properties of the latter can be 'homogenized' and treated as isotropic. Thus, we will treat this particle as homogeneous and isotropic, with properties to be determined by means of Chow's[20,21] method. In this consideration, the randomly wavy rod phase is approximated as spheres with a volume concentration of 0.23 in a topologically continuous PS matrix, as shown in *Figure 1b*. The results of averaging the elastic properties and the thermal expansion coefficient by Chow's method are listed in *Table 1* (see entry termed 'Homogenized' particle). The accuracy of this method, as applied to this morphology, has been discussed by one of us elsewhere[22]. The properties of the second type of particle are listed in *Table 1* as PB.

The third particle consists of concentric spherical shells of PB and PS (CS PB/PS), are shown in *Figure 2a*. It is composed of a collection of alternating layers of PB and PS block copolymer domains with elastic properties listed in *Table 1*. The volume ratio of PB to PS is 1/2, and is given by the molecular weight ratio of PB to PS in the block copolymer. It too is in a matrix phase of high molecular weight PS. This, of course, is a composite microstructure that cannot be homogenized and is analysed as a layered particle, as depicted in the schematic idealization shown in *Figure 2b*.

The fourth particle also consists of concentric spherical shells of PB and PS, with a morphology identical to that shown in *Figure 2*, but also incorporates additional low molecular weight PB (3 Kg mol^{-1}). It will be referred to here as the concentric-shell-low molecular weight polybutadiene/polystyrene particle (CS LMWPB/PS). The additional low molecular weight PB in this particle is dispersed in the PB spherical shells of the block copolymer, resulting in a smaller volume fraction of PS in the particle, and giving a volume ratio of PB to PS of 2/1

Table 1 Materials' properties

Materials	Bulk modulus (MPa)	Shear modulus (MPa)	Volumetric coefficient of thermal expansion ($°C^{-1}$)
PS	3.265 (10^3)	1.25 (10^3)	2.0 (10^{-4})
PB	1.938 (10^3)	0.62	7.5 (10^{-4})
LMWPB	1.938 (10^3)	0.31	7.5 (10^{-4})
Homogenized	2.880 (10^3)	0.88 (10^3)	3.07 (10^{-4})
H2	2.849 (10^3)	0.86 (10^3)	3.17 (10^{-4})

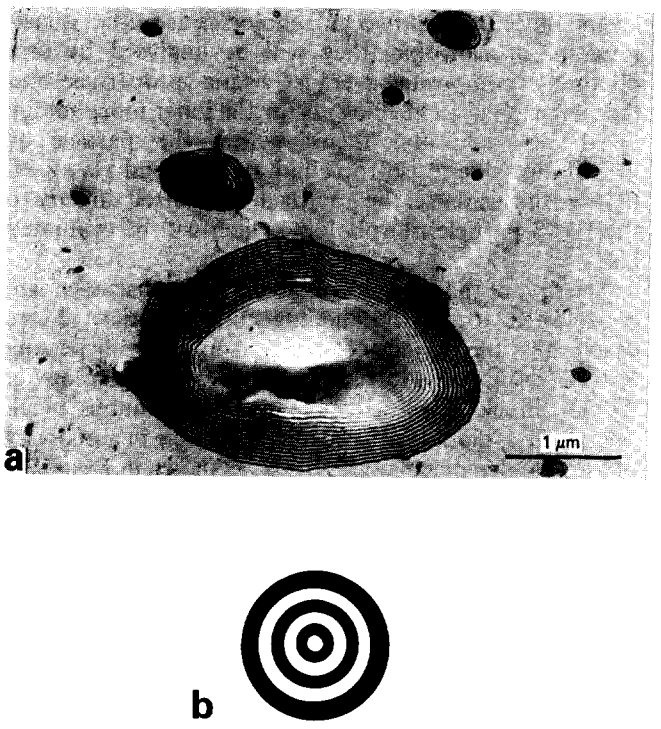

Figure 2 A concentric spherical shell particle incorporating additional low molecular weight PB, abbreviated as CS LMWPB/PS: (a) micrograph, (b) idealized morphology chosen for modelling purposes

among the concentric spherical shells. This particle is also surrounded by a matrix phase of high molecular weight PS. It is analysed in the same way as particle three above.

The fifth, high impact polystyrene (HIPS) particle having the well-known morphology shown in *Figure 1b*, where, however, the PS and PB phases are interchanged, will be treated by the same techniques used for the K-resin particle.

All of the particles are assumed to have a perfect bond between themselves and the surrounding PS matrix transmitting all tractions. This is a valid assumption because the particles are composed of block copolymers and therefore, there does exist a high concentration of primary chemical bonds acting across the interfaces of the PB and PS blocks, both inside the composite particles and along the eventual interface between particles and matrix. All these composite particles primarily exhibit elastic behaviour; however, the glassy PS matrix can also creep under sustained load and can undergo some viscoplastic stress relaxation as a result. This will be discussed later.

Stress histories

As mentioned above, each particle introduces a thermal expansion and stiffness misfit to the matrix. The magnitude of the misfits differ with each particle because both the morphology and the material composition of each particle can differ. These misfits induce stresses in the matrix around the particle, which in turn contribute to the initiation of crazes.

The thermal expansion misfit is introduced during the processing of the heterogeneous material. At the glass transition temperature of PS (95°C) both the PS and the PB should be fully relaxed and free of internal stress. All material is exposed to this temperature to remove unknown internal stresses due to the previous processing steps consisting of moulding or solvent casting followed by differential removal of solvent by evaporation and uneven cooling. We consider that material, bearing all five particles, has been cooled from T_g of PS to room temperature of 20°C at similar rates. The two components of the materials, i.e., the PB and PS, have very different coefficients of thermal expansion in the temperature range below 95°C, where PS acts as a stiff glassy solid, while PB acts as a lightly crosslinked rubber. This different behaviour induces a thermal misfit stress between the particle and the matrix, in order to maintain compatibility.

Subsequently, this thermal stress can be partially relaxed because of the non-linear creep behaviour in the PS matrix. It will be shown that for lengths of time of interest, this stress relaxation can sometimes be significant.

A second kind of misfit is introduced when an external stress is imposed on the material. In most cases, the stress of interest is an applied far field tensile stress. The misfit occurs because each component material, PB and PS, possesses different elastic properties, causing a non-uniform distribution of the stress in the matrix. The end result is a stress concentration around the particle, and particularly at the equatorial plane, as defined in *Figure 3*, but also secondarily at the poles.

STRESS ANALYSIS

Thermal residual stress

The thermal residual stresses developed in the matrix and the homogenized (isotropic) particle can be determined analytically from existing solutions for misfitting spheres. In order to include the effect of finite volume fractions of particles, the analysis considers two concentric spheres of radius a and b, as shown in *Figure 4*. The inner sphere represents the particle, and the outer shell represents the matrix allocated to one particle. The volume fraction of particles is $c=(a/b)^3$. Considering that no external stresses are applied, i.e., the radial stress acting across $r=b$ is zero, the interfacial radial stress resulting from the enforcement of compatibility between the particle and the matrix due to a temperature change of ΔT is:

$$\sigma_r=\frac{K_p(\gamma_m-\gamma_p)\,\Delta T}{1+\dfrac{1}{1-c}\dfrac{K_p}{K_m}\left[\dfrac{1+\nu_m}{2(1-2\nu_m)}+c\right]}=\sigma, \qquad (1)$$

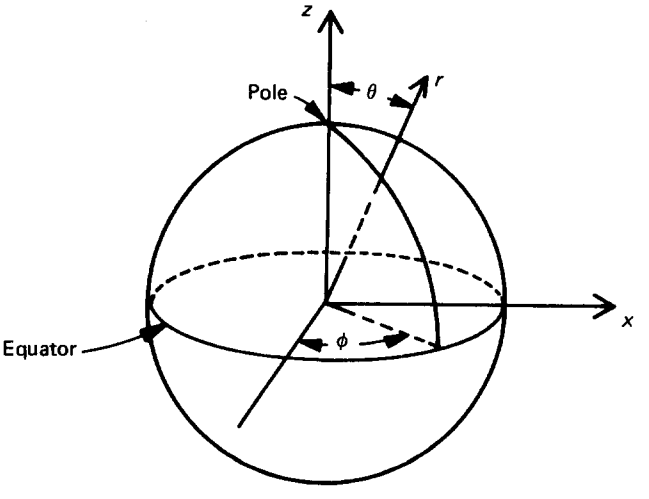

Figure 3 Coordinate axes for spherical particle

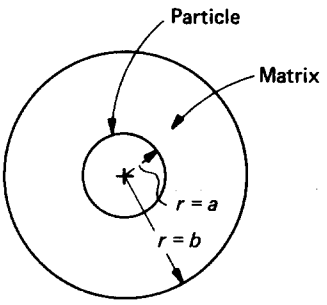

Figure 4 Idealization of a spherical particle in a finite volume fraction c, as two concentric spheres with radius ratio $a/b = c^{1/3}$

where K is the bulk modulus; γ is the volumetric coefficient of thermal expansion; and v is Poisson's ratio. The subscripts 'm' and 'p' stand for matrix and particle, respectively.

When the particle itself is heterogeneous, the effective bulk modulus K_p and the volumetric coefficient of expansion γ_p of the particle must be obtained first by treating it as a micro-composite. Such a treatment by the method of Chow[20,21] gives for an occluded phase of spherical shape

$$K_p = K_2\left\{1+\frac{\left[\frac{K_1}{K_2}-1\right]c_1}{1+\left[\frac{K_1}{K_2}-1\right][1-c_1]\left[\frac{1+v_2}{3(1-v_2)}\right]}\right\} \quad (2)$$

$$\gamma_p = \gamma_2\left\{1+\frac{\frac{K_1}{K_2}\left[\frac{\gamma_1}{\gamma_2}-1\right]c_1}{1+\left[\frac{K_1}{K_2}-1\right]\left[\left[1-c_1\right]\left[\frac{1+v_2}{3(1-v_2)}\right]+c_1\right]}\right\} \quad (3)$$

In equations (2) and (3), the subscripts 1 and 2 stand for the occluded phase of the spherical form, and the topologically continuous surrounding phase in the particle, respectively.

The resulting misfit stresses in the particle and in the surrounding matrix due to σ are, in spherical coordinates:

$$\text{Particle:}\quad \sigma_r = \sigma_\theta = \sigma_\phi = \sigma; \qquad (r \leqslant a) \quad (4a)$$

$$\text{Matrix:}\quad \sigma_r = \left[\left(\frac{a}{r}\right)^3 - c\right]\frac{\sigma}{1-c}; (a \leqslant r \leqslant b) \quad (4b)$$

$$\sigma_\theta = -\left[\frac{1}{2}\left(\frac{a}{r}\right)^3 + c\right]\frac{\sigma}{1-c}; (a \leqslant r \leqslant b) \quad (4c)$$

where r indicates radial position, θ and ϕ are the altitude and azimuthal angles, respectively.

When considering a particle in an infinite matrix, i.e., $c = 0$, the stresses at the interface reduce to:

$$\sigma = \frac{K_p(\gamma_m - \gamma_p)\Delta T}{1+\frac{K_p}{K_m}\frac{(1+v_m)}{2(1-2v_m)}};$$

$$\text{Particle:}\quad \sigma_r = \sigma_\theta = \sigma_\phi = \sigma \qquad (r \leqslant a) \quad (5a)$$

$$\text{Matrix:}\quad \sigma_r = \sigma\left(\frac{a}{r}\right)^3 \qquad (r \geqslant a) \quad (5b)$$

$$\sigma_\theta = \sigma_\phi = -\frac{\sigma}{2}\left(\frac{a}{r}\right)^3 \qquad (r \geqslant a) \quad (5c)$$

For this case only, the matrix stresses are purely deviatoric everywhere, and the negative pressure becomes zero in the matrix.

To obtain a closed-form solution for the stresses developed due to the thermal expansion misfit between the matrix and the third and fourth composite particles with concentric spherical shells is a lengthy and tedious task because of the multi-layered internal structure of the particle and the thermal misfit between the layers within the particle. However, a very good solution can easily be obtained with a finite element (FEM) analysis. Both the geometry and loading of the problem are spherically symmetric; therefore, only a small section of the problem needs to be considered. This section, with appropriate boundary conditions, is pictured in *Figure 5*. The finite element code ABAQUS was used in the analysis. The stress distribution within the particle, as well as in the matrix, was obtained. The accuracy of the solution was determined by conducting a finite element analysis on an isotropic particle and comparing the results with the analytical solution in the theory of elasticity, already discussed above. The error was found to be less than 1%.

The results of the analytical and FEM study indicate that the thermal stresses developed within the quasi-homogeneous (homogenized) K-resin and HIPS particles and the two concentric spherical shell particles differ dramatically. The homogenized particles develop a uniform hydrostatic stress, as shown by equation (4a). To obtain the magnitude of these hydrostatic stresses for particles in an infinite medium, i.e., for $c = 0$, for the two specific cases of the K-resin particle and the HIPS particle, the bulk moduli and coefficients of thermal expansion must be obtained from equations (2) and (3). For the K-resin particle $K_1/K_2 = K_{PB}/K_{PS}$, $\gamma_1/\gamma_2 = \gamma_{PB}/\gamma_{PS}$, $v_2 = v_{PS} = 0.33$, and $c_1 = 0.23$; while for the HIPS particle $K_1/K_2 = K_{PS}/K_{PB}$, $\gamma_1/\gamma_2 = \gamma_{PS}/\gamma_{PB}$, $v_2 = v_{PB} = 0.5$, and $c_1 = 0.8$ in most typical cases, as we will discuss below in a more detailed evaluation. This results in $K_p = 2.88$ GPa and $\gamma_p = 3.08 \times 10^{-4}$ K^{-1} for the K-resin particle and $K_p = 2.88$ GPa and $\gamma_p = 3.10 \times 10^{-4}$ K^{-1} for the HIPS particle. Thus, ignoring the small differences between the volumetric coefficients of expansion, these two particles have nearly identical bulk moduli and net coefficients of thermal expansion, apparently because the effect of their inverted topologies are nearly fully compensated by the somewhat different volume fractions of occluded phases. In an infinite PS matrix, the negative pressure inside the composite particles due to a thermal expansion misfit resulting from a temperature difference of $\Delta T = -75$ K is 7.95 MPa for both particles, for the component phase properties listed in *Table 1*.

The thermal loading produces a stress gradient in the two concentric shell particles, with the stresses increasing as the particle centre is approached. *Figure 6* shows the negative pressure gradient carried by the PB layers of

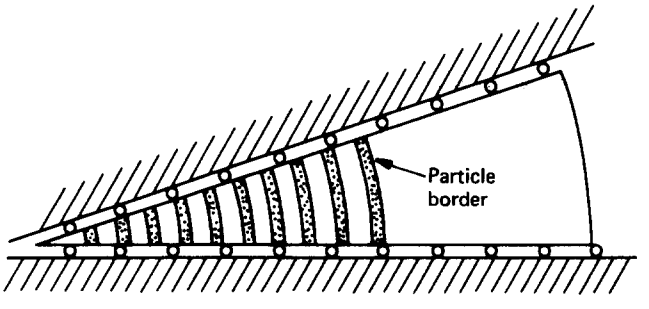

Figure 5 A characteristic 'slice' of a concentric spherical shell particle, as used to model the thermal expansion misfit problem

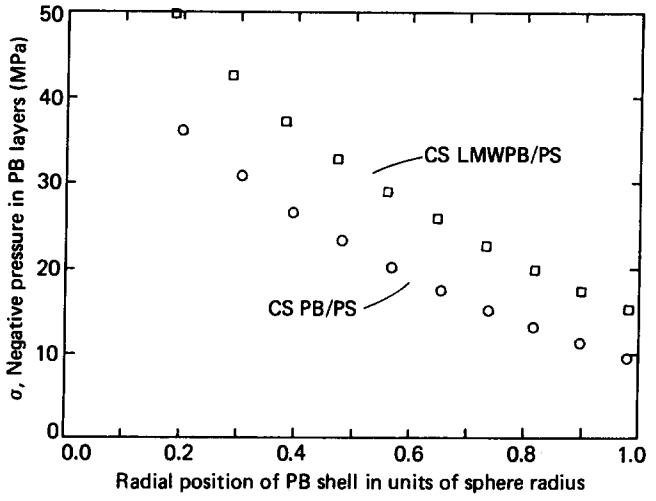

Figure 6 Negative pressure distribution in the PB shells of the CS PB/PS and CS LMWPB/PS particles induced by a thermal expansion misfit between 95°C and room temperature

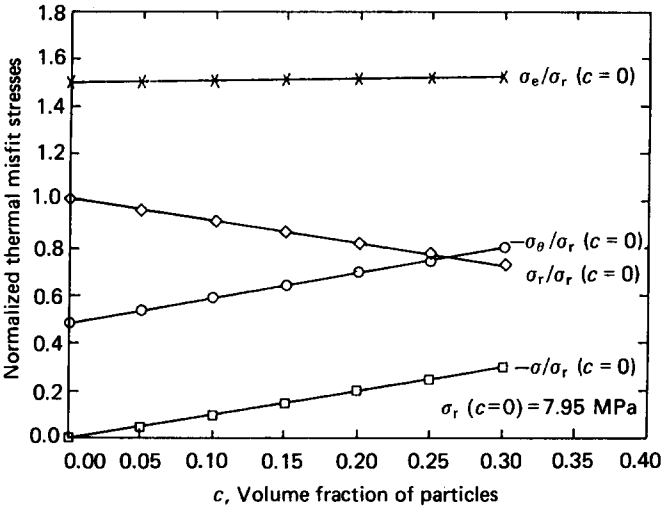

Figure 7 Effect of volume fraction c of particles on the thermal expansion misfit stresses in the matrix on the particle border, induced by the homogenized particle

both particles, each having a PS core and 10 concentric alternating PB and PS shells. The PS layers support a hoop stress σ_θ, as well as a negative pressure, and are instrumental in building up the negative pressure toward the centre. These stress levels are a maximum when the particles are in an infinite matrix. The resulting negative pressures in the PB layers for the CS PB/PS particle range from 10 MPa to 38 MPa from the particle border to the centre and that for the CS LMWPB/PS particle range from 14.9 MPa to 50 MPa in the particles with 10 concentric shells, both for a $\Delta T = -75°C$ and the properties listed in *Table 1*.

The stress state in the matrix at the particle/matrix interface is similar in trend for all particles. When the particle is in an infinite matrix, the stress state is purely deviatoric throughout the matrix. As the volume fraction of particles is increased, a positive pressure is developed in the surrounding matrix to compensate for the negative pressures inside the particles, while the deviatoric stress remains approximately the same. The matrix stresses which are highest at the particle border are shown in *Figure 7* for the two homogenized particles. The dependence of the normalized matrix stresses at the particle border on particle volume fraction is very similar for the other particles. The magnitudes of the stresses in an infinite matrix are shown in *Table 2* for all particles, which can be used as the scale factors for the finite volume fraction problems of *Figure 7*. The largest stresses in the realizable particles, result from the CS LMWPB/PS particle which gives a radial stress of 14.9 MPa at the particle border. The stress for the idealized pure PB particle is naturally, considerably higher at 34.5 MPa. This is not surprising because the CS LMWPB/PS particle is the one with the greatest percentage of PB, at 67%. The CS PB/PS particle possesses 33% PB, and resulted in a radial stress of 9.68 MPa, while the homogenized particle, containing 23% PB for the K-resin and 80% PS for HIPS, resulted in a radial stress of only 7.95 MPa at the particle border. However, it is not just the material composition which affects the thermal stress level, but also the microstructure of the particle, as is clear from the very different morphologies of the K-resin and HIPS particles. This effect is determined in a different way by considering a particle containing the same volume ratio of PB and PS as the CS PB/PS particle, but in a homogenized form (the H2 particle in *Table 1*) and calculating the thermal stresses produced by this particle. Such a particle would produce a radial thermal stress of 8.64 MPa when in an infinite matrix. This is more than 10% lower than the 9.68 MPa from the CS PB/PS particle. Therefore, we conclude that the concentric shell morphology produces a greater effective thermal expansion misfit than the homogenized morphology.

Uniform applied tension

Particles in an infinite matrix. For the present, we will neglect any linear or non-linear relaxation of the thermal residual stresses that may happen in the matrix material during sustained loading but we will consider what happens when an additional tensile stress is applied in the far field. A closed-form solution for this problem is available for an isotropic particle in an infinite medium, while finite element analyses were necessary for the concentric shell particles and finite matrix effects.

The stress distribution around a spherical elastic inhomogeneity in an infinite elastic matrix under a uniform far field tensile stress has been determined by Goodier[23]. His solution assumes the matrix and the particle to be homogeneous and isotropic, as well as perfectly bonded to one another. Therefore, this solution can be used for both cases of the homogenized particles, and the pure PB particle problems.

Table 2 Thermal residual stresses for particles in an infinite medium for $\Delta T = 75°C$

Particle	Particle stress σ_r (MPa)	Matrix stress at particle border	
		σ_r (MPa)	σ_θ (MPa)
Homogenized[a]	7.95	7.95	3.97
PB	34.5	34.5	−17.8
CS PB/PS[b]	—	9.68	−4.84
CS LMWPB/PS[b]	—	14.9	−7.45
H2	8.64	8.64	−4.32

[a] For both the K-resin particle and the HIPS particle
[b] Particles containing 10 concentric alternating spherical shells of PB and PS

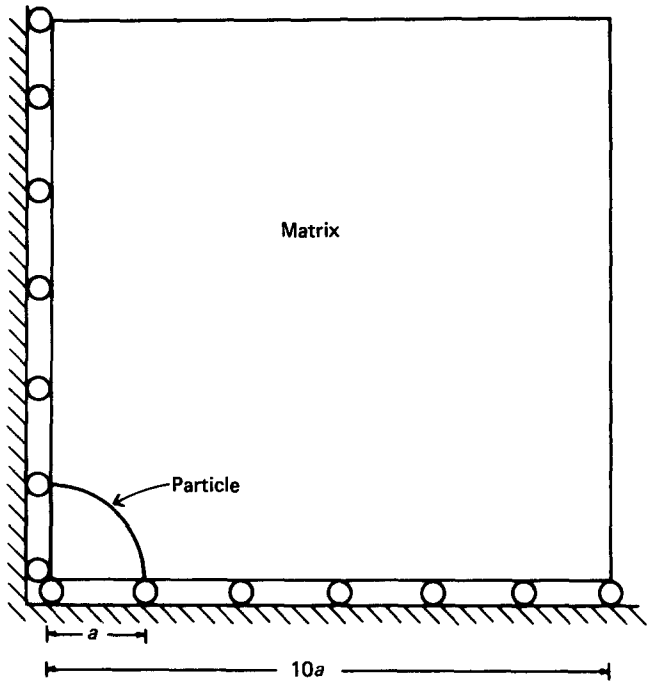

Figure 8 Geometry and boundary conditions for the FEM modelling of the concentric spherical shell particles. The rollers represent zero displacement normal to the line. For the inner structure of the particle, see *Figure 11*

A finite element analysis was conducted to determine the stress field around the concentric shell particles due to a uniform far field tensile stress. The axial symmetry of the geometry and loading are taken advantage of in the finite element modelling problem depicted in *Figure 8*, which shows the outer PS region. The detailed structure for the inside portion of the layered particle is shown in *Figures 11a, b* below. The accuracy of the FEM solution was determined by conducting a finite element analysis also for an isotropic particle and comparing the results with those of the Goodier solution. This indicated less than 3% error in the main stress concentration factor for the stress σ_θ at the equatorial plane.

The results for the homogeneous particles indicate that the elastic inhomogeneity effect of the particle with differing elastic properties from the matrix causes a non-uniform stress distribution with a range of about 4 particle radii in the region surrounding the particle upon the application of the far field tension[23] in the case of particles in an infinite medium. The distribution of stress in the matrix around the homogeneous particle has been given by Goodier[23] in spherical coordinates. This distribution is well known and will not be re-stated here. The state of stress inside the particle is homogeneous, according to Eshelby's[24] well-known generic solution of the ellipsoidal inhomogeneity problem.

The state of stress in the matrix outside the concentric spherical shell particles was obtained from the finite element solution. These stresses were compared with the distributions resulting from the Goodier solution for the homogeneous and homogenized particles. For the purpose of craze initiation, the individual components of the stresses are of less interest than the Mises equivalent stress and the negative pressure which enter the more physically based theoretical models directly[25-27]. The distribution of Mises equivalent stress and negative pressure in the surrounding matrix within a layer of one particle radius are given in *Figures 9a* and *9b*, for the homogenized K-resin particle. The results for the HIPS particle and the homogeneous PB particle are very similar, though quantitatively somewhat different. The corresponding results for the CS LMWPB/PS layered particle are given in *Figures 10a* and *10b*. Again, the results for the somewhat less flexible CS PB/PS particle are very similar, except, of course, the local stress concentrations are considerably less. In both cases, it is clear that both the Mises equivalent stress and the negative pressure are concentrated primarily around the equatorial region. There is a lesser concentration of Mises equivalent stress also at the poles. On the other hand, the concentration of the mean normal stress changes from a negative pressure

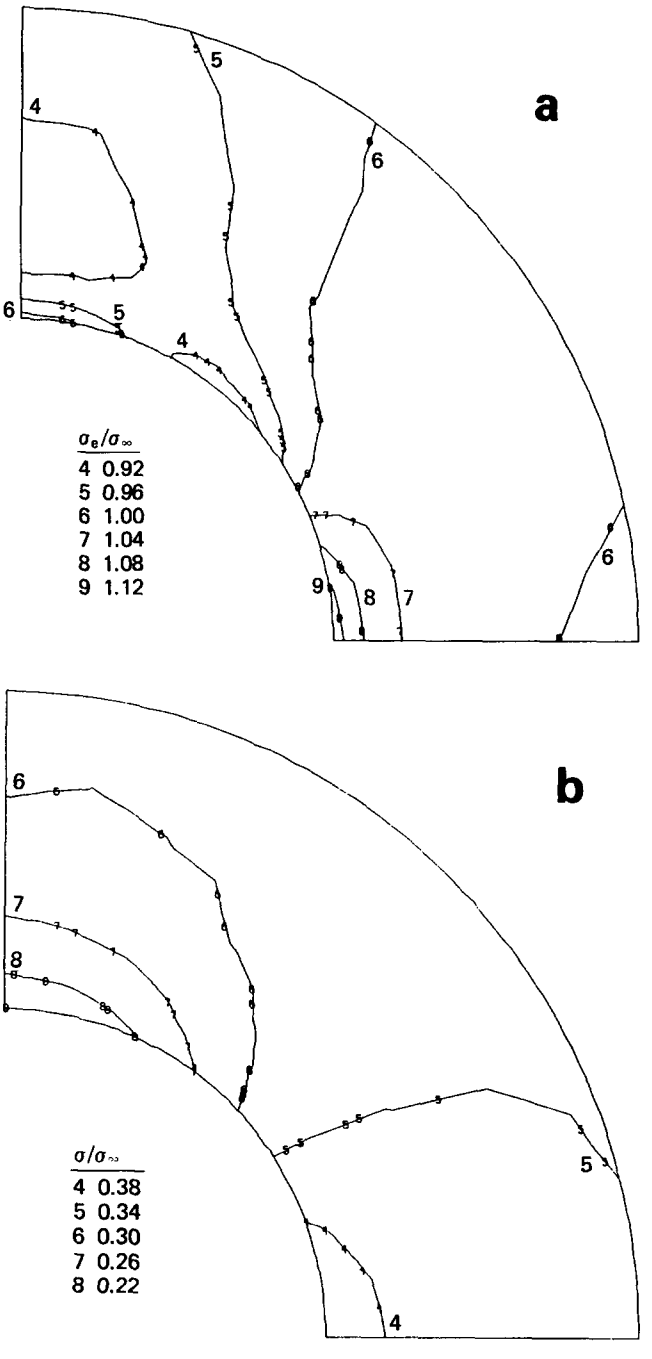

Figure 9 Distributions of stress in a matrix layer of one radius thickness around the homogenized particle: (a) equivalent stress σ_e, (b) negative pressure σ

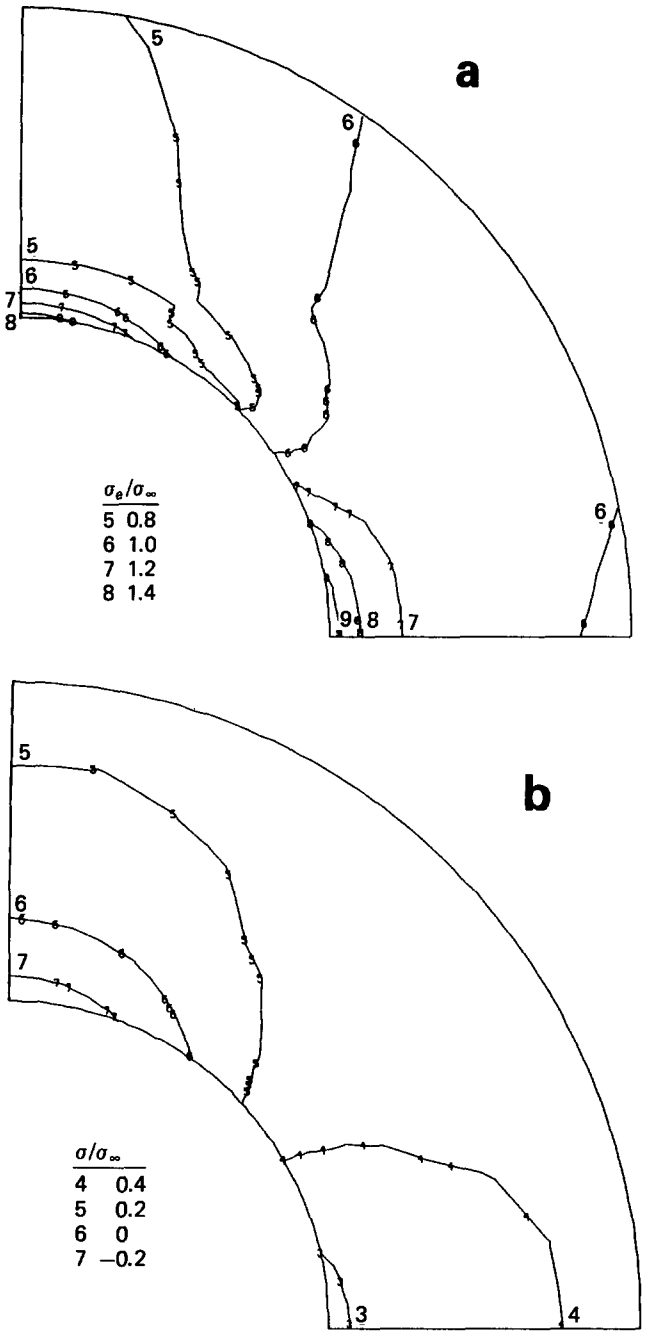

Figure 10 Distribution of stress in a matrix layer of one radius thickness around the CS LMWPB/PS particle: (a) equivalent stress σ_e, (b) negative pressure σ

along the equator, to a pressure at the poles. The actual concentrations of all the stresses individually, as well as the Mises equivalent stress σ_e and negative pressure σ are given in *Table 3*, for an equatorial point, in units of the distant tensile stress σ_∞ for all five particles.

In *Table 3*, the results are listed for particles in the order of increasing flexibility of the particle, from left to right. The pure PB particle represents the ultimate achievable performance with rubber, while the homogenized K-resin particle with its topologically continuous PS block phase is the least flexible of all. Clearly, the CS LMWPB/PS particle, which is the best one achievable with a high quality interface, has come quite close to the ultimate performance of the pure PB particle, which cannot be obtained in the micron size range with a high quality primary bond interface. Thus, in the CS LMWPB/PS particle, the concentration of tangential stress σ_θ, Mises equivalent stress σ_e, and negative pressure σ, have achieved 83.3, 90, and 72.6% of the performance difference between the poorest (homogenized K-resin) and the best (pure PB) particles. The performance of the homogenized particle may actually be somewhat better than depicted here. The stress concentrations for this particle are a lower bound estimate because the elastic properties of this particle were calculated by Chow's[21] method, which for this morphology, gives an answer close to an upper bound for stiffness. The HIPS particle appears slightly less effective than the CS PB/PS particle.

While the state of strain inside the homogeneous particles is homogeneous, as is well known from Eshelby's generic solution[24], the strain inside the layered particles is complex and intricate, as is shown in *Figures 11a* and *11b* for the case of the CS LMWPB/PS particle. In these Figures, the dotted contours represent the undistorted, ten concentric PB and PS layers of the particle modelled. Under a distant tensile stress, as the particle elongates in the direction of the tensile stress, the spherical PS layers merely flex, while the PB layers with their almost negligible shear moduli undergo fluid-like motions. The PB squeezed out from the equatorial plane 'flows' up toward the poles, where the differential flexure of the PS shells make more room for it in the annular gaps.

Particles of finite volume fractions. When the volume fraction of particles is finite, their zones of perturbation of the matrix interpenetrate, which serves to increase the magnitude of each component of stress. This has been investigated for a volume fraction of 0.21 that was of interest for the experimental system investigated by Gebizlioglu *et al.*[9]. In the model, regularly placed particles are considered in periodic axi-symmetric cells with periodic boundary conditions, where the stressed top face and free cylindrical side faces are displaced uniformly. Clearly, this constitutes an upper bound model for the interaction of the particles.

The result of this study for the CS LMWPB/PS particles is given in *Table 4*, comparing the concentrations of stress for a material with $c=0.21$ volume fraction of particles, with the case of these particles in infinite dilution, at $c=0$.

The interactions of homogeneous particles in a uniaxial tensile field has been solved earlier by Broutman and Panizza[16], also by the finite element method in a way very similar to the procedure described above, but for a series of increasing volume fractions. For completeness of

Table 3 Equatorial stress state in matrix outside particle, due to applied tension, σ_∞, in infinite medium

Equatorial stress	Homogenized	CS PB/PS	CS LMWPB/PS	PB
σ_r/σ_∞	0.050	0.039	0.130	0.286
$\sigma_\theta/\sigma_\infty$	1.160	1.690	1.760	1.880
$\sigma_\phi/\sigma_\infty$	0.008	0.054	0.046	0.040
σ_e/σ_∞ [a]	1.130	1.640	1.670	1.730
σ/σ_∞ [b]	0.407	0.594	0.645	0.735

[a] σ_e is the Mises equivalent stress
[b] σ is negative pressure (mean normal stress)

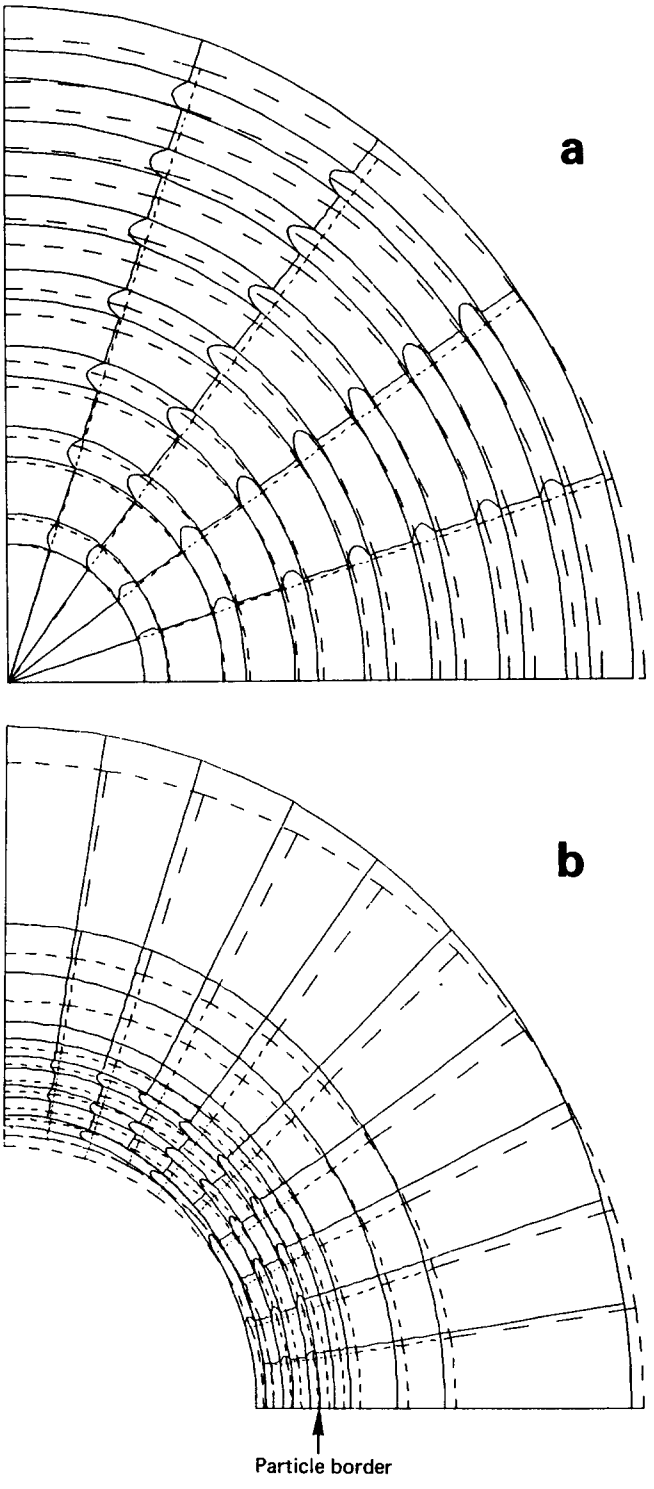

Figure 11 Flow-like distortions in the PB layers of a CS LMWPB/PS particle under a distant tensile stress: (a) inner 7 layers of PB, displacement magnification factor is 105; (b) outer 3 layers of PB and part of the surrounding PS matrix, displacement magnification factor is 162

presentation, we have reproduced their principal results in *Figure 12*. Inspection of their results indicates that significant increases in stress levels do not occur among homogeneous particles until particle volume fractions exceed 0.3. Since usual volume fractions of particles in heterogeneous polymer systems are approximately in the range of 0.2, including those in the experiments of Gebizlioglu *et al.*[8,9] that are being modelled here, this interaction effect will not be dramatic. In HIPS, however, the particle volume fraction can often be as high as 0.5, making consideration of particle interactions necessary. The result for the layered particles shown in *Table 4* is generally in agreement with *Figure 12*.

In most cases, the particles are likely to be randomly distributed in the volume in a real polymer, resulting in larger local variations in volume fraction than the average of 0.2 that is of interest. Thus, early craze initiation should be expected from such regions. The prematurely initiated crazes in these regions, however, should level down the local elevation of stress so that the average particle size and spacing is still likely to govern the overall behaviour, by arguments similar to upper bounds to limit loads in plastically deforming structures[28].

RELAXATION OF THERMAL STRESSES

It must be recognized that the thermal stresses in the majority phase of PS surrounding the composite particles are set up in the final cooling process from the last annealing step at 100°C, and will remain applied for long

Table 4 Finite matrix effects on stress concentrations around the CS LMWPB/PS particles for two volume fractions of particles

Equatorial stresses	$c=0$	$c=0.21$
σ_r/σ_∞	0.130	0.158
$\sigma_\theta/\sigma_\infty$	1.760	1.88
$\sigma_\phi/\sigma_\infty$	0.046	0.100
σ_e/σ_∞ [a]	1.670	1.750
σ/σ_∞ [b]	0.645	0.713

[a] σ_e is the Mises equivalent stress
[b] σ is negative pressure (mean normal stress)

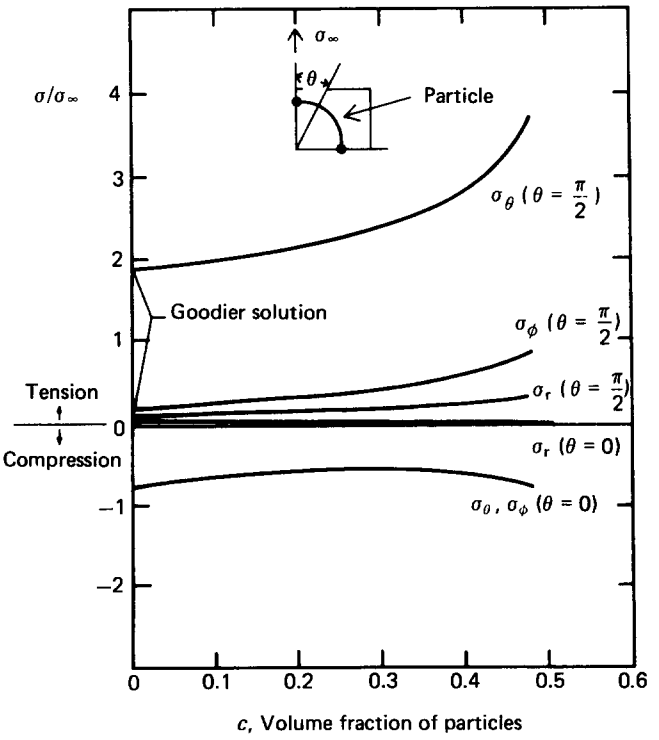

Figure 12 Dependence of the equatorial stresses and pole stresses around a particle on the volume fraction of particles. [Reproduced from Broutmann, L. J. and Panizza, G. *International Journal of Polymeric Materials* 1971, **1**, 95, by permission of Gordon and Breach Science Publishers]

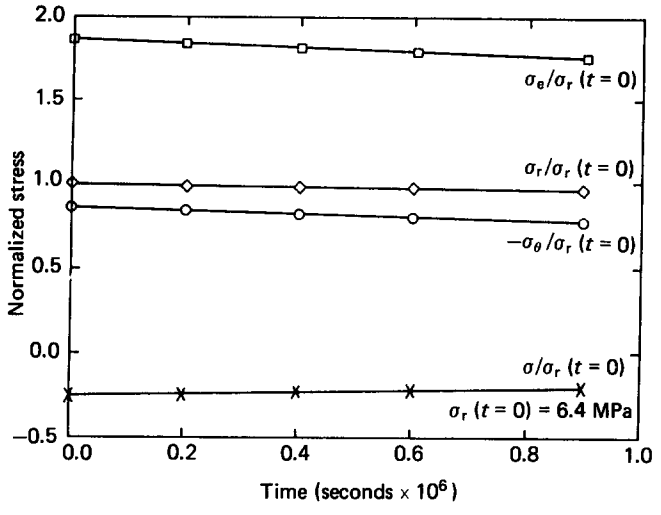

Figure 13 Viscoplastic relaxation of thermal residual stresses in the PS matrix around a homogenized particle, for a particle volume fraction of 0.2

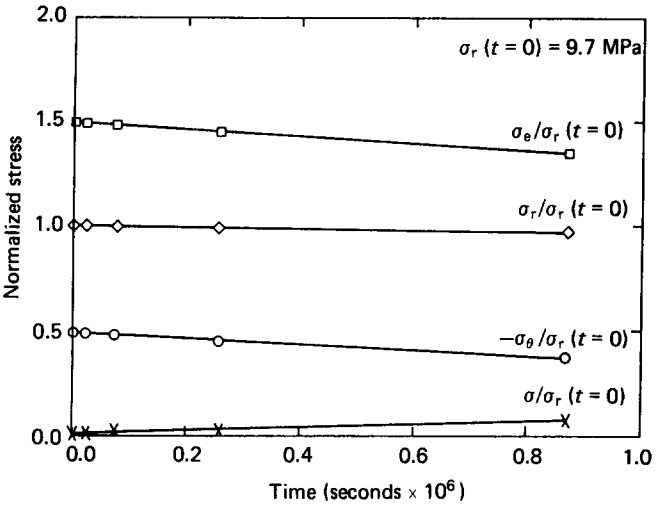

Figure 14 Viscoplastic relaxation of thermal residual stresses in the PS matrix around a CS PB/PS particle in an infinite domain

periods of time at room temperature until the samples are tested or otherwise used. Thus, it is possible that considerable stress relaxation can occur in the PS over this initial period of 'sitting on the shelf.' Linear viscoelastic stress relaxation at room temperature in PS should be too low to be of much importance. There is little information on the stress relaxation of PS in the appropriate non-linear stress range at room temperature. Therefore, we model this behaviour as viscoplastic relaxation by the plastic flow theory of Argon and Bessonov[29], in which the equivalent inelastic shear strain rate can be written as:

$$\dot{\gamma} = \dot{\gamma}_0 \exp[-\Delta G^*/kT] \tag{6}$$

with an activation-free enthalpy, ΔG^*, given by:

$$\Delta G^* = \frac{3\pi\mu\omega^2 a^3}{16(1-\nu)}[1 - 8.5(1-\nu)^{5/6}(\sigma_e/3^{1/2}\mu)^{5/6}] \tag{7}$$

In equation (7), μ, ω, a, are the average shear modulus, average rotation angle of a molecular segment producing the local shear relaxation and, a, the segment radius. The details of this theory have been experimentally verified by Argon and Bessonov, and are not a subject of discussion here. We adopt its form and use the experimental constants of Argon and Bessonov in our evaluation.

The analysis of the relaxation of the thermal residual stresses around the composite particles in our materials is quite lengthy and is summarized in the Appendix. The stress relaxation results at room temperature for the K-resin particle and the two concentric shell particles (all in an infinite matrix) are shown in *Figures 13–15*. These indicate that there is very little relaxation of the stresses surrounding the K-resin particle and the CS PB/PS particles over a period of *ca.* 10^6 s at room temperature, but a much greater relaxation of stresses around the CS LMWPB/PS particle. This, of course, is due to the higher deviatoric stress around the CS LMWPB/PS particle produced by the much larger thermal expansion misfit of this particle.

DISCUSSION

Craze initiation in a uniform stress field

The principal purpose of evaluating the mechanical properties of the four composite particles and the PB particle, which we have presented and analysed in the preceding sections, was to compare the effectiveness of different morphologies in craze initiation.

Many *ad-hoc* uniaxial stress or strain criteria for craze initiation have been proposed by early investigators which have been evaluated by Wang *et al.*[30] for application under multi-axial conditions and have been found of little predictive value. The first multiaxial craze initiation criterion with any generality was proposed by Sternstein and Ongchin[31] on the basis of biaxial craze initiation experiments on poly(methyl methacrylate) (PMMA). Other multi-axial craze initiation criteria have been put forward by Oxborough and Bowden[10], Argon and Hannoosh[25], and by Kawagoe and Kitagawa[27], to mention only the most prominent. The last two authors have also re-evaluated all existing multiaxial crazing criteria for specific application to cases of solvent crazing. They found that only the criterion of Argon–Hannoosh had the proper form that permitted modification to successfully account for their experiments on solvent effects. Their own alternative criterion differed only insignificantly from that of Argon and Hannoosh[25]. Therefore, we will consider only this criterion in craze

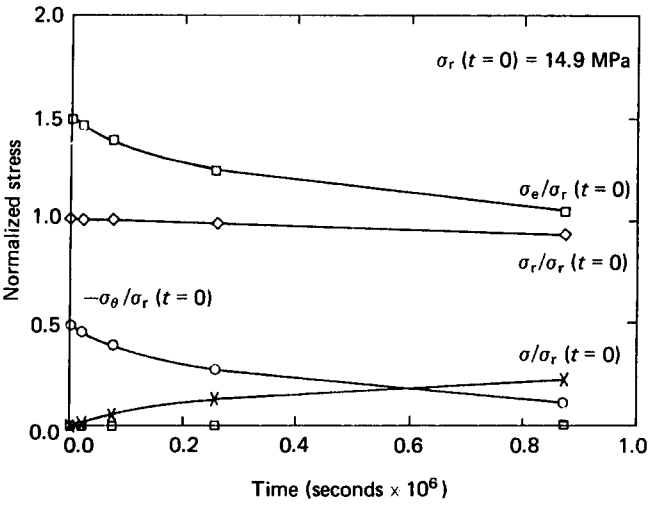

Figure 15 Viscoplastic relaxation of thermal residual stresses in the PS matrix around a CS LMWPB/PS particle in an infinite domain

Table 5 Equatorial stress state due to thermal stresses and applied tension σ_∞ (in MPa)

(a) Infinite matrix

Particle	Homogenized	CS PB/PS	CS LMWPB/PS
Stress (MPa):σ_r	$7.95+0.05\sigma_\infty$	$9.68+0.04\sigma_\infty$	$14.9+0.13\sigma_\infty$
σ_θ	$-3.97+1.16\sigma_\infty$	$-4.84+1.69\sigma_\infty$	$-7.45+1.76\sigma_\infty$
σ_ϕ	$-3.97+0.01\sigma_\infty$	$-4.84+0.54\sigma_\infty$	$-7.45+0.046\sigma_\infty$
σ	$0.41\sigma_\infty$	$0.594\sigma_\infty$	$0.645\sigma_\infty$
σ_e	$[142-12.8\sigma_\infty+1.28\sigma_\infty^2]^{1/2}$	$[211-24.2\sigma_\infty+2.70\sigma_\infty^2]^{1/2}$	$[500-34.6\sigma_\infty+2.80\sigma_\infty^2]^{1/2}$

(b) Finite matrix

Particle	Homogenized ($c=0.22$)	CS LMWPB/PS ($c=0.21$)
Stress (MPa):σ_r	$6.41+0.1\sigma_\infty$	$11.47+0.158\sigma_\infty$
σ_θ	$-5.64+1.314\sigma_\infty$	$-10.13+1.88\sigma_\infty$
σ_ϕ	$-5.64+0.02\sigma_\infty$	$-10.13+0.10\sigma_\infty$
σ	$-1.62+0.478\sigma_\infty$	$-2.93+0.713\sigma_\infty$
σ_e	$[145-13.7\sigma_\infty+1.58\sigma_\infty^2]^{1/2}$	$[467+35.9\sigma_\infty+3.07\sigma_\infty^2]^{1/2}$

Table 6 Equatorial stress state due to thermal stresses (after an 8 day relaxation period at 300 K) and applied tension σ_∞ (in MPa)

(a) Infinite matrix

Particle	Homogenized	CS PB/PS	CS LMWPB/PS
Stress (MPa) σ_r	$7.76+0.05\ \sigma_\infty$	$9.42+0.04\ \sigma_\infty$	$13.8+0.13\ \sigma_\infty$
σ_θ	$-3.5+1.16\ \sigma_\infty$	$-3.6+1.09\ \sigma_\infty$	$-1.81+1.76\ \sigma_\infty$
σ_ϕ	$-3.5+0.08\ \sigma_\infty$	$-3.6+0.054\ \sigma_\infty$	$-1.81+0.046\ \sigma_\infty$
σ	$0.25+0.41\ \sigma_\infty$	$0.74+0.594\ \sigma_\infty$	$3.39+0.645\ \sigma_\infty$
σ_e	$[127-12.9\ \sigma_\infty+1.20\ \sigma_\infty^2]^{1/2}$	$[170-21.6\ \sigma_\infty+2.70\ \sigma_\infty^2]^{1/2}$	$[244-24.1\ \sigma_\infty+2.80\ \sigma_\infty^2]^{1/2}$
β (during relaxation)	~ 0	~ 0	$0(10^{-18})$

(b) Finite matrix

Particle	Homogenized ($c=0.22$)	CS LMWPB/PS ($c=0.21$)
Stress (MPa) σ_r	$6.24+0.1\ \sigma_\infty$	$10.6+0.158\ \sigma_\infty$
σ_θ	$-5.04+1.314\ \sigma_\infty$	$-5.42+1.88\ \sigma_\infty$
σ_ϕ	$-5.04+0.02\ \sigma_\infty$	$-5.42+0.1\ \sigma_\infty$
σ	$-1.28+0.478\ \sigma_\infty$	$-0.08+0.713\ \sigma_\infty$
σ_e	$[127-12.8\ \sigma_\infty+1.58\ \sigma_\infty^2]^{1/2}$	$[257-26.7\ \sigma_\infty+3.07\ \sigma_\infty^2]^{1/2}$
β (during relaxation)	~ 0	$0(10^{-18})$

initiation. In the Argon and Hannoosh model, crazes initiate in two stages. In the first and precursor stage, a concentration of molecular level porosity β increases linearly with time t in a thermally activated way, in response to the deviatoric component σ_e (equivalent tensile stress) of the stress tensor, i.e., as

$$\beta = C_1 t \exp(-C_2/\sigma_e), \tag{8}$$

where $C_1 = 1.66 \times 10^7\ s^{-1}$ and $C_2 = 1.65$ GPa at 300 K, as determined from bi-axial craze initiation experiments on polystyrene. In the second stage, this porosity expands plastically under the combined action of the negative pressure σ and deviatoric stress σ_e, according to the well-known generalized yield response of porous plastic continua[32,33]. This gives rise to an initiation condition of

$$\sigma = Q(\beta, \sigma_e/Y)\frac{2Y}{3}\ln(1/\beta) \tag{9}$$

where Q is the symbolic representation of this generalized yield condition for the plastic expansion of the pores, and Y is the plastic resistance in tension[25]. The value of Q in equation (9) will be taken to be equal to 1.33×10^{-2} on the basis of Argon and Hannoosh's evaluation, while $Y = 70$ MPa at 300 K.

The local deviatoric stress σ_e and negative pressure σ around the particle is affected by both the thermal expansion misfit and the applied far field tension in qualitatively different ways. Thus, although the contributions of these two stimuli to the individual stresses at an equatorial material element can be superimposed, the equivalent stresses have to be calculated separately. To start with, it is necessary to first determine the fixed level of the thermal misfit stresses which depend only on the temperature difference between T_g and the observation temperature, and then combine these with the stresses produced by the distant tension. This has been done for the K-resin particle and the two concentric shell particles for their known coefficient of expansion misfit and for a distant tensile stress σ_∞.

The computed individual total stress components σ_r, σ_θ, σ_ϕ, as well as the total deviatoric stress σ_e and negative pressure σ are given in *Table 5* for both an infinite matrix and a finite matrix, but for no viscoplastic stress relaxation. The effects of the viscoplastic relaxation on the thermal misfit stresses and the consequences of that are given in *Table 6*, to parallel the information in *Table 5*. The term β in *Table 6* represents the calculated levels of protoporosity at the end of the precursor stage.

Comparison of the crazing effectiveness of particles

We now compare the craze initiation effectiveness of the five particles discussed above under the action of an external stress σ_∞ alone in an infinite matrix, without regard of the thermal misfit stresses present in the particles. This comparison is not quite on equal ground, since the different particles contain different volume fractions of PB. While it is readily possible to normalize the results by calculating the properties of the four composite particles for a common volume fraction of PB, this would still not permit comparison of these with the pure PB particle.

The sought craze initiating effectiveness of particles will be based on the criterion given in equation (9).

For the comparison that we seek, we define a dimensionless rate R of crazing as

$$R=\frac{1}{C_1 t}=\exp\left[\frac{3(\sigma_\infty/Y)}{2Q}\left(\frac{\sigma}{\sigma_\infty}\right)-\frac{(C_2/Y)}{(\sigma_\infty/Y)(\sigma_e/\sigma_\infty)}\right] \quad (10)$$

which is obtained from equations (8) and (9) with a little further modification. Equation (10) can be used for direct substitution of the local equatorial stresses around the five particles given in *Table 3* for the five particles. Considering the pure PB particle as the ultimate in performance, we define a reference figure of merit for each particle as the ratio of the dimensionless crazing rate of that particle to the dimensionless rate for the PB particle, evaluated at a typical applied stress level σ_∞/Y. The calculated figures of merit for the five particles at a typical stress level $\sigma_\infty/Y=0.2$ are given in *Table 7*. They show that the two concentric spherical shell particles are much better than the HIPS particle, and that in comparison to these three, the particle of pure KRO-1 resin is orders of magnitude worse. The pure PB particle is the best performer in every respect.

In calculating the stress concentrations around the HIPS particle, typical conditions that prevail for such particles were considered. Thus, e.g., from dynamic shear modulus measurements of a pure PS and a HIPS sample at room temperature, moduli of 1.25 GPa and 0.57 GPa are found, respectively[1]. The modulus for the HIPS sample is for a volume fraction of 0.1 of PB and a volume fraction of 0.8 of occluded PS in the particles[1]. This gives a composite particle volume fraction of 0.5 in the HIPS, and permits determination of the effective shear modulus and Poisson's ratio of the composite particles as 0.156 GPa and 0.489 respectively at room temperature through the use of Chow's method[20]. The specific stress concentrations listed in *Table 3* were then obtained from Goodier's results[23].

Table 7 Comparison of figures of merit for craze initiation for all particles at a stress level $\sigma_\infty/Y=0.2$

Homogenized K-resin	HIPS	CS PB/PS	CS LMWPB/PS	PB
1.05×10^{-20}	2.80×10^{-5}	9.89×10^{-4}	1.11×10^{-2}	1

Comparison with experiments

As a final application of our developments, we now use the deviatoric stresses and negative pressures determined from our analysis, and listed in *Table 5* above, to develop some understanding of the recent experimental observations of Gebizlioglu *et al.*[8,9] on the homogenized particles and the concentric spherical shell particles.

With the information given in the preceding section above, the required tensile stress σ_∞ to initiate crazes around the equatorial region of a particle within a typical time under load of, say 10^2 s, was calculated for the K-resin particle and the two concentric shell particles, taking initially no note of stress relaxation. The combined stress state due to thermal stress and the applied tension σ_∞ for each of these particles is listed in *Tables 5a* and *5b* for infinite and finite matrices, respectively. The calculated results for σ_∞ are shown in the first row of *Table 8*. Comparing these results with the experimental results given in the last row, we notice that the correct trend is predicted, i.e., the concentric spherical shell particles, CS PB/PS, will initiate crazes at a lower applied stress level than the homogenized particle, and of these, the modified particle CS LMWPB/PS gives the lowest stress. However, the magnitudes of the predicted stresses are substantially higher than the experimental results. This could be due to the neglect of the relaxation of the thermal stresses. The relaxation of these stresses can aid the craze initiation process in two ways. Firstly, the relaxation of the deviatoric stresses outside the particle by viscoplastic flow should result in the establishment of some microporosity, β. Secondly, the stress relaxation also lowers the level of the detrimental 'image' pressure that is present between particles to compensate for the negative pressure inside the particle for finite volume fraction of particles. Both of these effects were considered by using the relaxed values of local stress given in *Tables 6a* and *6b* to calculate σ_∞. The calculated levels of σ_∞ for these relaxed thermal stresses are given in *Table 8* in the second row. Apart from the CS LMWPB/PS particle, the effect of viscoplastic stress relaxation was slight, and resulted in negligible changes, as is clear from *Table 8*.

The above analysis supports the conclusion of Gebizlioglu *et al.*[9], that new factors are at play and that separate considerations are necessary to explain the very low levels of craze flow stresses reported by these authors, as well as those that have been accepted for HIPS for

Table 8 Tensile stresses, σ_∞, for craze initiation

		Homogenized		CS PB/PS	CS LMWPB/PS	
		$c=0$	$c=0.22$	$c=0$	$c=0$	$c=0.21$
σ_∞ (MPa)	Unrelaxed	36	33	26	24	24
	Relaxed[a]	36	33	25	22	22
	Experimental[b]	—	30	10	—	10

[a] For an 8 day relaxation period
[b] Gebizlioglu *et al.*[8,9]

many years. Clearly, the stress analysis presented above leaves little uncertainty about the stress state around the particles. Even though larger spherical shell particles with more layers result in ever increasing levels of thermal negative pressure in the centre of the particle, the effect on the particle border is far less dramatic. Considering that perhaps the various craze initiation constants C_1, C_2, Q, etc., reported by Argon and Hannoosh for PS may be suspect, more uncompromising upper bound analyses were also performed for viscoplastic cavitation of a porous plastic continuum using the generalized cavitation loci of Gurson[32] to calculate craze initiation stresses based on 'first principles' which gave even less satisfactory agreement with experiments[22].

Thus, we are led to conclude that the reported craze flow stresses of Gebizlioglu *et al.*[9] were not directly governed by initiation of crazes from particles. In fact, their observations and our analysis indicate that in those experiments, crazes must have resulted from the particle interfaces, not by a homogeneous nucleation process, as studied by Argon and Hannoosh[25] in homo-PS, but by a heterogeneous nucleation process at fairly low stresses. The nature of this heterogeneous nucleation process is unclear. Additional local stress concentrations are difficult to identify, and there is little evidence from the known nature of the particle interfaces[34] to expect an embryonic morphology with the properties of craze microstructure. This suggests that the subject craze flow stress appears to have been governed by the growth of crazes against an unusually low plastic resistance in the craze matter tufts. That this must have been the case, can be confirmed by some simple dimensional considerations.

As has been discussed in some detail by Argon *et al.*[7], the kinematic considerations of a craze dilatation rate $d\theta/dt$ on planes normal to the applied tensile stress σ_∞ result in an average tensile strain rate

$$\dot{\varepsilon}_\infty = \frac{d\theta}{dt} = (2b_f\theta_{cr})\left(\frac{2\pi an}{V}\right)\frac{da}{dt}, \tag{11}$$

where $2b_f$ is the primordial thickness of a craze, and θ_{cr} the dilatation inside a mature craze. The second term $(2\pi an/V)$, has been identified as the active craze front length per unit volume, while da/dt is the velocity of a craze front under a distant tensile stress of σ_∞. Thus, if the active craze front length per unit volume is not governed by a nucleation consideration, it must be of a strictly geometrical origin related to the number density of particles. We consider here for simplicity, a planar, two-dimensional model of the situation where this term can be taken to be about two active craze fronts per projected area $(2\bar{b})^2$ per particle on the vertical plane of observation, of an average particle. Thus,

$$\frac{2\pi an}{V} \rightarrow \frac{2}{(2\bar{b})^2} = \frac{8c}{\pi\bar{d}^2} \tag{12}$$

where $\bar{d}$ is taken as the 'size average' particle diameter for the concentric shell particles, of a total volume fraction c. Then the required average craze velocity to produce a tensile strain rate $\dot{\varepsilon}_\infty$ is simply

$$\frac{da}{dt} = \frac{\pi\bar{d}^2\dot{\varepsilon}_\infty}{8c(2b_f\theta_{cr})}. \tag{13}$$

Taking $\bar{d} = 3.2\times10^{-6}$ m, $c = 0.22$, $2b_f\theta_{cr} = 3\times10^{-6}$ m, as representative values in the experiments of Gebizlioglu *et al.*[9], and previous considerations of Argon *et al.*[7], we calculate an average required craze front velocity of 7.92×10^{-10} cm s^{-1}. Using the normalized stress dependence of craze velocity at 300 K in PS published by Argon and Salama[35], we determine a required level of $\sigma_\infty/\hat{Y}$ of 0.110, where $\hat{Y}$ is the athermal flow stress in PS at 300 K[29], which can be taken as 278 MPa from theoretical considerations[29,35]. This gives a required tensile stress σ_∞ of only 31.5 MPa, which, however, is still more than a factor 3 higher than the experimental value of 10 MPa. Hence, we must conclude that the effective athermal plastic resistance $\hat{Y}$ of the craze tufts must have been less than 1/3 of the value in bulk, to explain the low craze flow stresses of Gebizlioglu *et al.*[9]. That this may indeed be the case emerges from new cyclic stressing experiments of Gebizlioglu *et al.*[36] of extensively crazed blends containing concentric spherical shell particles which demonstrate very substantial retraction behaviour upon unloading.

It is interesting to note that these same considerations must apply also to HIPS, which has craze flow stresses usually no higher than 13–15 MPa.

Our analysis further shows that the most effective particles for craze initiation should be composed of pure rubber, as this would have the largest thermal expansion misfit and the highest compliance. For them to be useful, however, they have to be grafted to the surrounding matrix. This consideration also applies to a cavity which produces the maximum local stress concentration, but is totally ineffective in toughening because it constitutes also an initial defect of super-critical size for fracture inside any craze that it might initiate.

CONCLUSIONS

The craze initiating effectiveness of composite particles of rubber and stiff glassy polymers depend on both their thermal expansion misfit and their tensile compliance.

Both the thermal expansion misfit-induced negative pressure inside a particle and the tensile stress-induced load shedding of the particle to its surroundings contribute effectively to the deviatoric stress at the particle border. On the other hand, while the thermal misfit produces an 'image' pressure outside the particle, the load shedding produces a negative pressure along the equator of the particle.

Viscoplastic relaxation of the thermal stress outside the particles can reduce the 'image' pressure, somewhat, while it produces deviatoric inelastic strains that are known to result in protoporosity. Thus, such relaxation promotes crazing.

The best estimates of the stress enhancing effects of particles in recent experiments on block copolymer particles of concentric spherical shell morphology, and in HIPS indicate that it is unlikely that their craze flow stresses are governed by craze initiation from particles. Rather, the results indicate that craze initiation is not an important barrier, and that the flow stresses are governed by craze growth.

ACKNOWLEDGEMENT

This research has been supported by the MRL Division of NSF under Grant DMR-84-18718, through the Center for Materials Science and Engineering at the Massachusetts

Institute of Technology. We are grateful to our colleagues Professor R. E. Cohen and Dr O. S. Gebizlioglu, for many useful discussions.

REFERENCES

1 Bucknall, C. B., 'Toughened Plastics', Applied Science Publishers, London, 1977
2 Rabinowitz, S. and Beardmore, P., in 'Critical Reviews in Macromolecular Science', Eds E. Baer *et al.* CRC Press, Cleveland, Ohio (1972), Vol 1, p 1
3 Kambour, R. P. *J. Polym. Sci., Macromol. Rev.* 1973, **7**, 1
4 Kramer, E. in 'Advances in Polymer Science', Ed. H. H. Kausch, Springer Verlag, Berlin (1983), Vol. 52/53, p 1
5 Dettenmaier, M. in 'Advances in Polymer Science', Ed. H. H. Kausch, Springer Verlag, Berlin (1983), Vol. 52/53, p 57
6 Kawai, H., Hashimoto, T., Miyoshi, K., Ono, H. and Fujimura, M. *J. Macromol. Sci.-Phys.* 1980, **B17**, 427
7 Argon, A. S., Cohen, R. E., Gebizlioglu, O. S. and Schwier, C. E. in 'Advances in Polymer Science', Ed. H. H. Kausch, Springer Verlag, Berlin (1983), Vol. 52/53, p 275
8 Gebizlioglu, O. S., Argon, A. S. and Cohen, R. E. *Polymer* 1985, **26**, 519
9. Gebizlioglu, O. S., Argon, A. S. and Cohen, R. E. *Polymer* 1985, **26**, 529
10 Oxborough, R. J. and Bowden, P. B. *Phil. Mag.* 1974, **30**, 171
11 Pavan, A. and Ricco, T. *J. Mater. Sci.-Lett* 1976, **11**, 1180
12 Ricco, T., Pavan, A. and Dannsso, F. *Polym. Eng. Sci.* 1978, **18**, 774
13 Pavan, A. in 'Role of Polymer Matrix in Processing and Structural Properties of Composite Materials', Eds. J. C. Seferis and L. Nicolais, Plenum Press, New York (1983), p 523
14 Bocij, H. C. *Polymer* 1977, **18**, 47
15 Arends, C. B., unpublished Dow Chemical Company Report (1976)
16 Broutmann, L. J. and Panizza, G. *Int. J. Polym. Mater.* 1971, **1**, 95
17 Molau, G. E. and Wittbrodt, W. H. *Macromolecules* 1968, **1**, 260
18 Kruse, R. L. *Polym. Prepr.* 1977, **18**(1), 838
19 Argon, A. S., Cohen, R. E., Jang, B. Z. and Vander-Sande, J. B. in 'Toughening of Plastics', Plastics and Rubber Institute, London (1978), p 16-1
20 Chow, T. S. *J. Polym. Sci. Polym. Phys. Edn.* 1978, **16**, 959
21 Chow, T. S. *J. Polym. Sci. Polym. Phys. Edn.* 1978, **16**, 967
22 Boyce (née-Cunningham), M. E., 'Craze Initiation in Heterogeneous Polymers', *S.M. Thesis*, Dept. Mech. Eng., MIT (1983)
23 Goodier, J. N. *ASME Trans.* 1933, **55**, 39
24 Eshelby, J. D. *Proc. Roy. Soc. Lond.*, 1957, **A241**, 376
25 Argon, A. S. and Hannoosh, J. G. *Phil. Mag.* 1977, **36**, 1195
26 Ishikawa, M., Narisawa, I. and Ogawa, H. *J. Polym. Sci. Polym. Phys. Edn.* 1977, **15**, 1791
27 Kawagoe, M. and Kitagawa, M. *J. Polym. Sci. Polym. Phys. Edn.* 1981, **19**, 1423
28 McClintock, F. A. and Argon, A. S. 'Mechanical Behavior of Materials', Addison Wesley, Reading, Mass. (1966), p 359
29 Argon, A. S. and Bessonov, M. I. *Phil. Mag.* 1977, **35**, 917
30 Wang, T. S., Matsuo, M. and Kwei, T. K. *J. Appl. Phys.* 1973, **42**, 547
31 Sternstein, S. S. and Ongchin, L. *Polym. Prepr.* 1969, **10**, 117
32 Gurson, A. L. *J. Eng. Mater. Tech.* 1977, **99**, 2
33 McClintock, F. A. and Stowers, I. F., Res. Memo. No. 159 (Fatigue and Plasticity Laboratory, M.E. Dept., MIT, Cambridge, Mass.)
34 Bates, F. S., Berney, C. V. and Cohen, R. E. *Macromolecules* 1983, **16**, 1101
35 Argon, A. S. and Salama, M. M. *Phil. Mag.* 1977, **36**, 1217
36 Gebizlioglu, O. S., Argon, A. S. and Cohen, R. E. to be published

APPENDIX

Relaxation of residual stresses

A solution is sought for the stresses, as they relax around a spherical particle of radius a due to the creep behaviour of the matrix which surrounds the particle in the form of a concentric sphere of radius b, as approximated in *Figure 4*. To obtain this solution, basic kinematics will be considered first. One can write the total strains in the matrix around the particle as the sum of elastic, thermal, and creep strains:

$$\varepsilon_r = \varepsilon_r^e + \varepsilon_r^T + \varepsilon_r^c;$$

$$\varepsilon_\theta = \varepsilon_\theta^e + \varepsilon_\theta^T + \varepsilon_\theta^c;$$

$$\varepsilon_\phi = \varepsilon_\theta.$$

where $\varepsilon_i^c = \int_t \dot{\varepsilon}_i^c \, dt$, and $\varepsilon_\phi = \varepsilon_\theta$ because the problem is spherically symmetric. The thermal strains are considered to be imposed initially by cooling from T_g of the matrix material to room temperature, where they set up an initial thermal strain which remains constant with time. Therefore, if we work in terms of strain rates, the total strain rate may be written as:

$$\dot{\varepsilon}_r = \dot{\varepsilon}_r^e + \dot{\varepsilon}_r^c; \tag{A1a}$$

$$\dot{\varepsilon}_\theta = \dot{\varepsilon}_\theta^e + \dot{\varepsilon}_\theta^c; \tag{A1b}$$

$$\dot{\varepsilon}_\phi = \dot{\varepsilon}_\theta; \tag{A1c}$$

because the thermal strain rate is zero. Introducing the elastic stress–strain relation, the strain rates may be written as:

$$\dot{\varepsilon}_r = \frac{1}{E}[\dot{\sigma}_r - 2\nu\dot{\sigma}_\theta] + \dot{\varepsilon}_r^c; \tag{A2a}$$

$$\dot{\varepsilon}_\theta = \frac{1}{E}[(1-\nu)\dot{\sigma}_\theta - \nu\dot{\sigma}_r] + \dot{\varepsilon}_\theta^c. \tag{A2b}$$

These can be rewritten to give expressions for the stress rates as a function of the total strain rate and the creep strain rate:

$$\dot{\sigma}_r = \frac{E}{(1-2\nu)(1+\nu)}[(1-\nu)(\dot{\varepsilon}_r - \dot{\varepsilon}_r^c) + 2\nu(\dot{\varepsilon}_\theta - \dot{\varepsilon}_\theta^c)]; \tag{A3a}$$

$$\dot{\sigma}_\theta = \frac{E}{(1-2\nu)(1+\nu)}[(\dot{\varepsilon}_\theta - \dot{\varepsilon}_\theta^c) + \nu(\dot{\varepsilon}_r - \varepsilon_r^c)]. \tag{A3b}$$

Now, in order to obtain expressions for $\dot{\varepsilon}_r^c$ and $\dot{\varepsilon}_\theta^c$ in terms of the known effective creep rate expression $\dot{\varepsilon}^c$, which in our case is taken as the Argon–Bessonov expression, as given by equations (6) and (7), the assumption of material incompressibility during creep flow is first introduced:

$$2\dot{\varepsilon}_\theta^c + \dot{\varepsilon}_r^c = 0$$

$$\dot{\varepsilon}_r^c = -2\dot{\varepsilon}_\theta^c.$$

Then, the definition of effective strain rate is used to relate the effective rate to the radial rate:

$$\dot{\varepsilon}_e = \left[\tfrac{2}{3}\dot{\varepsilon}_{ij}\dot{\varepsilon}_{ij}\right]^{1/2}; \tag{A4a}$$

$$\dot{\varepsilon}^c = \pm\dot{\varepsilon}_r^c = -\pm 2\dot{\varepsilon}_\theta^c. \tag{A4b}$$

The appropriate signs are determined by the deviatoric stress state. In this case, the initial radial deviatoric stress is positive, and the initial tangential deviatoric stress are negative. This results in:

$$\dot{\varepsilon}^c = +\dot{\varepsilon}_r^c = -2\dot{\varepsilon}_\theta^c \tag{A5}$$

Substituting equation (A5) into equations (A3) will yield expressions for the stress rates in terms of the total strain

rates and the effective creep rate:

$$\dot{\sigma}_r = \frac{E}{(1-2\nu)(1+\nu)}[(1-\nu)\dot{\varepsilon}_r + 2\nu\dot{\varepsilon}_\theta - (1-2\nu)\dot{\varepsilon}^c]; \tag{A6a}$$

$$\dot{\sigma}_\theta = \frac{E}{(1-2\nu)(1+\nu)}[\dot{\varepsilon}_\theta + \nu\dot{\varepsilon}_r + \tfrac{1}{2}(1-2\nu)\dot{\varepsilon}^c] \tag{A6b}$$

The total strain rates are still unknown and are found from the equilibrium equations. This problem is spherically symmetric, and therefore, only one equation remains to be satisfied:

$$\frac{d\dot{\sigma}}{dr} + \frac{2(\dot{\sigma}_r - \dot{\sigma}_\theta)}{r} = 0. \tag{A7}$$

This can be rewritten in terms of the strain rates through the use of equation (A6) and a relation between radial strains and tangential strains for spherically symmetric problems, $\dot{\varepsilon}_r = \dot{\varepsilon}_\theta + r\,d\dot{\varepsilon}_\theta/dr$. The resulting equilibrium equation, written in terms of the total unknown tangential strain rate and the known creep strain rate, is:

$$4\frac{d\dot{\varepsilon}_\theta}{dr} + r\frac{d^2\dot{\varepsilon}_\theta}{dr^2} = \frac{1-2\nu}{1-\nu}\left[\frac{d\dot{\varepsilon}_c}{dr} + 3\frac{\dot{\varepsilon}_c}{r}\right]. \tag{A8}$$

This may be multiplied by r^3 and rearranged to yield:

$$\frac{d}{dr}\left[r^4\frac{d\dot{\varepsilon}_\theta}{dr}\right] = \frac{(1-2\nu)}{(1-\nu)}\frac{d}{dr}[r^3\dot{\varepsilon}^c]. \tag{A9}$$

Equation (A9) can be integrated twice to obtain an expression for $\dot{\varepsilon}_\theta$:

$$\dot{\varepsilon}_\theta = \frac{1-2\nu}{1-\nu}\left[\int_a^r \frac{1}{r}\dot{\varepsilon}^c\,dr - a^3\dot{\varepsilon}^c(a)\left[\frac{1}{3a^3} - \frac{1}{3r^3}\right]\right]$$

$$+ a^4\left(\frac{d\dot{\varepsilon}_\theta}{dr}\right)_{r=a}\left[\frac{1}{3a^3} - \frac{1}{3r^3}\right] + \dot{\varepsilon}_\theta(a) \tag{A10}$$

By collecting unknown constant coefficients and assigning symbols to known expressions for simplicity,

$$C_1 = a^4\left(\frac{d\dot{\varepsilon}_\theta}{dr}\right)_{r=a};\quad C_2 = \frac{a}{3}\left(\frac{d\dot{\varepsilon}_\theta}{dr}\right)_{r=a} + \dot{\varepsilon}_\theta(a); \tag{A11,12}$$

$$A = \dot{\varepsilon}^c(a); \qquad I(r) = \int_a^r \frac{1}{r}\dot{\varepsilon}^c\,dr; \tag{A13, 14}$$

the total strain rates can be written as:

$$\dot{\varepsilon}_\theta = \frac{1-2\nu}{1-\nu}\left[I(r) - \frac{A}{3}\left(1 - \frac{a^3}{r^3}\right)\right] - \frac{C_1}{3r^3} + C_2; \tag{A15}$$

$$\dot{\varepsilon}_r = \frac{1-2\nu}{1-\nu}\left[I(r) + \dot{\varepsilon}^c - \frac{A}{3}\left(1 + 2\frac{a^3}{r^3}\right)\right] + \frac{2}{3}\frac{C_1}{r^3} + C_2. \tag{A16}$$

In order to obtain expressions for the unknowns C_1 and C_2, the appropriate boundary conditions must be applied. For the particle in a finite body, these conditions are:

at $r=a$, $\dot{\sigma}_r = \dot{\sigma}_p$; (A17)

at $r=a$, $\dot{u}_r = \dot{u}_p$; (A18)

at $r=b$, $\dot{\sigma}_r = 0$. (A19)

It is noted here that to obtain the solution for the particle in an infinite body, b is replaced by infinity and the solution is greatly simplified.

Applying boundary condition (A17) yields:

$$\frac{\dot{\sigma}_p}{E} = \left[\frac{2}{3a^3(1+\nu)}C_1 + \frac{C_2}{1-2\nu} - \frac{A}{1+\nu}\right]. \tag{A20}$$

Examining the expression for displacement at $r=a$, one can obtain an expression for $\dot{u}_p$ in terms of $\dot{\sigma}_p$:

$$u_p = \alpha_p \Delta T a + \frac{\sigma_3}{3K_p}a; \tag{A21}$$

$$\dot{u}_p = \frac{\dot{\sigma}_p}{3K_p}a; \tag{A22}$$

$$\dot{\sigma}_p = 3K_p\dot{\varepsilon}(a). \tag{A23}$$

where K_p is the effective bulk modulus of the particle. Combining boundary condition (A18) and equation (A22) yields:

$$\frac{\dot{\sigma}_p}{E} = \frac{R}{1-2\nu_p}\left[-\frac{C_1}{3a^3} + C_2\right]. \tag{A24}$$

where R is the ratio of the particle Young's modulus to the matrix Young's modulus, $R = E_p/E$. By equating equations (A20) and (A24), an expression for C_2 in terms of C_1 is obtained

$$\frac{R}{1-2\nu_p}\left[-\frac{C_1}{3a^3} + C_2\right] = \frac{2}{3a^3(1+\nu)}C_1 + \frac{C_2}{1-2\nu} - \frac{A}{1+\nu}$$

or

$$C_2 = \frac{(1-2\nu_p)(1-2\nu)}{R(1-2\nu)-(1-2\nu_p)} \times\left[C_1\frac{2(1-2\nu_p)+R(1+\nu)}{3a^3(1-2\nu_p)(1+\nu)} - \frac{A}{1+\nu}\right]. \tag{A25}$$

Applying boundary condition (A19) yields an expression for C_1 in terms of C_2:

$$C_1 = \frac{3b^3}{2}\left[-I(b)\frac{1+\nu}{1-\nu} + \frac{A}{3(1-\nu)}(1+\nu+2\nu(1-c)) - C_2\frac{1+\nu}{1-2\nu}\right] \tag{A26}$$

where $c=(a/b)^3$. Substituting equation (A25) into equation (A26) results in:

$$C_1 = \frac{3b^3}{2}\left[-I(b)\frac{1+\nu}{1-\nu} + \frac{A}{3(1-\nu)}(1+\nu+2\nu(1-c)) - \frac{(1+\nu)(1-2\nu_p)}{R(1-2\nu)-(1-2\nu_p)} \times\left[C_1\frac{2(1-2\nu_p)+R(1+\nu)}{3a^3(1-2\nu_p)(1+\nu)} - \frac{A}{1+\nu}\right]\right]. \tag{A27}$$

By grouping constant terms together,

$$Q = R(1-2\nu)-(1-2\nu_p), \tag{A28}$$

$$M = 2(1-2\nu_p)+R(1+\nu), \tag{A29}$$

$$F = 1+\nu+2c(1-2\nu), \tag{A30}$$

the unknown C_1 can be found to be:

$$C_1=\frac{3Qa^3}{2cQ+M}\left[-I(b)\frac{1+v}{1-v}+A\left[\frac{F}{3(1-v)}+\frac{1-2v_p}{Q}\right]\right]; \tag{A31}$$

and the unknown C_2:

$$C_2=\frac{(1-2v_p)(1-2v)}{Q}\times\left[C_1\frac{M}{3a^3(1-2v_p)(1+v)}-\frac{A}{(1+v)}\right]. \tag{A32}$$

Therefore, by substituting equations (A31) and (A32) into equations (A15) and (A16), the total strain rates are found. By substituting equations (A15) and (A16) into the stress rate expressions (A6a and b), we have the solution for the stress rate due to creep of the matrix.

Finally, the stress as a function of time is found by numerically integrating, using a forward Euler time integration scheme:

$$t+\Delta t_{\sigma_r}=t_{\sigma_r}+t_{\dot{\sigma}_r\Delta t}. \tag{A33}$$

The time increment, Δt, is chosen such that the maximum creep strain increment does not exceed a certain percentage (PCT) of the elastic strain;

$$\Delta t\leqslant(PCT)\varepsilon^e/\dot{\varepsilon}_c. \tag{A34}$$

Also, the integral $I(r)$ must be numerically integrated. This is done with a simple trapezoidal integration. The radial positions for this integration are chosen based upon the initial curve of $\dot{\varepsilon}_c(r)$.